Chemosphere 262 (2021) 128072

Contents lists available at ScienceDirect

Chemosphere

journal homepage: www.elsevier.com/locate/chemosphere

Polymer-assisted modification of metal-organic framework MIL-96 (Al): influence of HPAM concentration on particle size, crystal morphology and removal of harmful environmental pollutant PFOA

Luqman Hakim Mohd Azmi [a, b, c], Daryl R. Williams [c], Bradley P. Ladewig [a, d, *]

[a] Barrer Centre, Department of Chemical Engineering, Imperial College London, South Kensington Campus, SW7 2AZ, London, United Kingdom
[b] Grantham Institute – Climate Change and the Environment, Imperial College London, South Kensington Campus, SW7 2AZ, London, United Kingdom
[c] Surfaces and Particle Engineering Laboratory (SPEL), Department of Chemical Engineering, Imperial College London, South Kensington Campus, SW7 2AZ, London, United Kingdom
[d] Institute for Micro Process Engineering (IMVT), Karlsruhe Institute of Technology, Hermann-von-Helmholtz-Platz 1, 76344, Eggenstein-Leopoldshafen, Germany

HIGHLIGHTS

- Addition of HPAM during MIL-96 synthesis facilitated particle size enlargement.
- HPAM also functions as a crystal shape modifying agent.
- HPAM-grafted MIL-96 showed improvement in PFOA uptake quantity.

GRAPHICAL ABSTRACT

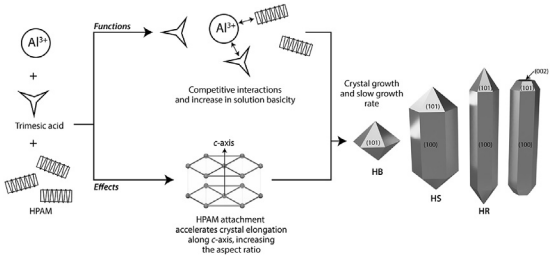

ARTICLE INFO

Article history:
Received 29 June 2020
Received in revised form
17 August 2020
Accepted 19 August 2020
Available online 22 August 2020

Handling Editor: Y. Yeomin Yoon

Keywords:
HPAM
Particle size
Crystal morphology
Metal-organic frameworks
Perfluorooctanoic acid
Adsorption

ABSTRACT

A new synthesis method was developed to prepare an aluminum-based metal organic framework (MIL-96) with a larger particle size and different crystal habits. A low cost and water-soluble polymer, hydrolyzed polyacrylamide (HPAM), was added in varying quantities into the synthesis reaction to achieve >200% particle size enlargement with controlled crystal morphology. The modified adsorbent, MIL-96-RHPAM2, was systematically characterized by SEM, XRD, FTIR, BET and TGA-MS. Using activated carbon (AC) as a reference adsorbent, the effectiveness of MIL-96-RHPAM2 for perfluorooctanoic acid (PFOA) removal from water was examined. The study confirms stable morphology of hydrated MIL-96-RHPAM2 particles as well as a superior PFOA adsorption capacity (340 mg/g) despite its lower surface area, relative to standard MIL-96. MIL-96-RHPAM2 suffers from slow adsorption kinetics as the modification significantly blocks pore access. The strong adsorption of PFOA by MIL-96-RHPAM2 was associated with the formation of electrostatic bonds between the anionic carboxylate of PFOA and the amine functionality present in the HPAM backbone. Thus, the strongly held PFOA molecules in the pores of MIL-96-RHPAM2 were not easily desorbed even after eluted with a high ionic strength solvent (500 mM NaCl). Nevertheless, this simple HPAM addition strategy can still chart promising pathways to impart judicious control over adsorbent particle size and crystal shapes while the introduction of amine functionality onto the surface chemistry is simultaneously useful for enhanced PFOA removal from contaminated aqueous systems.

* Corresponding author. Institute for Micro Process Engineering (IMVT), Karlsruhe Institute of Technology, Hermann-von-Helmholtz-Platz 1, 76344, Eggenstein-Leopoldshafen, Germany.
E-mail address: bradley.ladewig@kit.edu (B.P. Ladewig).

https://doi.org/10.1016/j.chemosphere.2020.128072
0045-6535/

1. Introduction

Adequate, clean and safe water supply is indispensable to healthy wellbeing of humans and living organisms (Tiedeken et al., 2017). Unfortunately, our surface and ground waters continue being polluted by industrial waste streams containing toxic and persistent chemicals including perfluorinated compounds (PFCs). PFCs have recently received much attention because they are ubiquitous contaminants in water, wildlife, and humans. The most commonly found PFCs in surface waters are perfluorooctanoic acid (PFOA) and perfluorooctane sulfonate (PFOS) (Rivera-Utrilla et al., 2013). Surprisingly, thus far, there is no mutually agreed international drinking water standard for PFOA and PFOS, but the United States Environmental Protection Agency have recommended a strict combined concentration limit of 70 ng/L (Cordner et al., 2019). Recent analysis of global water samples even revealed concentrations exceeding the provisional threshold (Andersson et al., 2019; Feng et al., 2020; Li et al., 2018; Lorenzo et al., 2019; Scher et al., 2018; Valsecchi et al., 2017).

Although most fluorochemical manufacturers have ceased their production of PFOA and PFOS in the early 2000s, this measure does not address the legacy pollution caused by these compounds (Wang et al., 2017). The ubiquitous presence and long-range mobility of PFCs is attributed to the high chemical stability of their C—F bonds (bond dissociation energy, $D^{\circ}_{298\ K} = 485$ kJ/mol) (Richardson, 2008), rendering them suitable as ingredients to make fluoropolymers (McNamara et al., 2018), fire-fighting foams (Cordner et al., 2019), and stain-repellent products (Richardson, 2008). Typical contamination hot spots then include the vicinity of industrial areas, military training sites, airports and wastewater treatment plants (Hu et al., 2016). Moreover, exposures to PFCs adversely affect body immunity (Sunderland et al., 2019), neurological functions (Piekarski et al., 2020), reproductive systems (Rashtian et al., 2019), as well as giving strong correlations to coronary heart disease (Huang et al., 2018), and cancer (Mancini et al., 2020) among many others. As a result, there is an urgent need to investigate efficient materials for PFCs remediation from contaminated water.

Of the treatments available for PFCs removal from water (Ateia et al., 2019), adsorption is extensively used given its simplicity, relatively lower cost and high selectivity (Du et al., 2014). Studied adsorbents range from activated carbon (AC) (Du et al., 2015; Xu et al., 2020), minerals (Shih and Wang, 2013; Wang and Shih, 2011), magnetic nanoparticles (Badruddoza et al., 2017), polymers (Xiao et al., 2017), resins (Yang et al., 2018), functionalized cellulose (Ateia et al., 2018), graphene oxide-silica hybrid (Ali et al., 2020), and metal-organic frameworks (MOFs) (Chen et al., 2016; Jun et al., 2019; Liu et al., 2015b; Sini et al., 2018, 2019). However, except for MOFs, most adsorbents only exhibit between low and moderate PFOA uptake compared to the industrial AC standard (>90% removal, 3 M Company, USA) (Vecitis et al., 2009).

MOFs refer to a novel class of porous materials made from organic bridging linkers and metal atoms. Distinguishing MOF features include their high surface areas, ready structure tunability and reusability via simple washing procedures which means that these materials are seen as a promising future substitute for AC (Xue et al., 2016). These features are befitting to resolve long-standing problems in PFOA removal by other conventional wastewater treatments especially given their dilute levels existence, low molecular weight, and high transportability (Chen et al., 2020; Gagliano et al., 2020). Further to that, in commercial water purification processes, adsorbents are generally deployed into a packed bed for continuous filtration. Fluids flowing through some packed beds may at times result in high pressure drops. This directly increases the energy requirement to pump the fluid through the bed and decreases the operational lifetime of the pumps, impacting on the economics of the process (Gebald et al., 2019). Although various factors are involved in optimal bed design, lowering the pressure drop can be easily achieved by increasing the adsorbent particle size (Mandic et al., 2017). Larger particles also facilitate easier recovery in between the washing cycles.

Size and crystal morphology of MOFs can be precisely controlled via the presence of additives (Seoane et al., 2016) such as initiation solvents (Liu et al., 2015a; Long et al., 2011), coordination modulators or capping agents (Guo et al., 2018; Han et al., 2015; Wang et al., 2013), surfactants (Falcaro et al., 2011), and hard templates (Yan et al., 2015) or through synthetic techniques using pyrolysis (Lee and Kwak, 2017), ultrasound (Vaitsis et al., 2019), and microreactor (Watanabe et al., 2017). Some complexities regarding the respective methods are usage of harmful organic solvents, use of acidic or basic modulators that increase risk of safety hazards and difficulty in isolating the hard templates after preparation. Whilst these three MOF synthetic techniques can only be carried out with specialized instrument, a common limitation of these approaches is the formation of predominantly nanoparticle products. The work reported here uses a surfactant-assisted method which serves as a multifaceted approach; functioning as a nanoreactor, a capping agent as well as a molecular template (Seoane et al., 2016).

The current study highlights a new one-pot surfactant-based synthesis method to control particle size and morphology of MOF crystals by utilizing a synthetic polymer, hydrolyzed polyacrylamide (HPAM). HPAM is a low cost and water-soluble polymer widely used for enhanced oil recovery in petroleum drilling processes, as well as being used as a flocculant for wastewater treatment (Rellegadla et al., 2017) where its benign effects on water quality are noted (Edomwonyi-Otu and Adelakun, 2018). Finally, a non-toxic and hydrothermally stable aluminum-based MOF, MIL-96 (Al) was chosen to be tested for liquid phase adsorption of PFOA. Given the positive surface charge for MIL-96 (Azhar et al., 2018), HPAM must be anionic to initiate particle aggregation. Such polymer-MOF composite strategy may also improve separation selectivity (Chang et al., 2020). In this case, the PFOA adsorption performance by the modified material was benchmarked with a commercial AC to understand the interaction mechanisms better.

2. Materials and methods

2.1. Chemicals

Polyacrylamide (PAM) (FLOPAM FA 920 SH, non-ionic, molecular weight (M_w) = 10—12 MDa) and partially hydrolyzed polyacrylamide (HPAM) (FLOPAAM FP 3630 S, anionic, 25—35 mol% hydrolyzed, $M_w = 18$ MDa) were supplied by SNF Floerger (France). Polyacrylic acid sodium salt (PAA, average M_w~2100), 2,2,2-trifluoroethanol (TFE, 99.5%), perfluorooctanoic acid (PFOA, 95%), ammonium acetate (AA, 99.0%), trimesic acid (TMA, 95%), sodium chloride (NaCl, 99%) were purchased from Sigma Aldrich. Deuterium oxide (D_2O, 99.9%) and aluminum nitrate nonahydrate ($Al(NO_3)_3 \cdot 9H_2O$, 98%) were purchased from Fluorochem and Alfa Aesar respectively. All other chemicals and solvents were reagent grade and used without further purification. Ultrapure water (H_2O) used throughout the study was obtained from PureLab Chorus ELGA unit. Granular activated carbon (AC) F400 was procured from Chemviron Carbon as a high-grade, steam-activated bituminous coal.

2.2. ^{19}F NMR analysis

Concentration for the internal standard (TFE) solution was set to 2.3 mM by transferring 0.42 mL TFE into 1 L H_2O. The NMR analyte

consists of 0.25 mL D_2O, 0.25 mL filtrate and 0.2 mL TFE. Quantification was performed according to the literature (Sini et al., 2018). Integrated area under the characteristic peaks of the terminal CF_3 groups for PFOA (−80 ppm) was compared relative to the TFE peaks (−76 ppm). Residual PFOA concentration after adsorption was calculated from the linear calibration equation obtained.

2.3. Adsorption

Prior to adsorption, the adsorbents were activated overnight at 120 °C under vacuum. All sorption experiments were conducted at room temperature. A PFOA stock solution (1000 mg/L) was prepared using ultrapure H_2O. The adsorbent (20 mg) was added with 20 mL PFOA solution into a screw cap vial, stirred for 72 h and then, the solution was filtered. The filtrate was collected for NMR analysis while the filtered solids were reused for desorption. The experiments were performed in duplicate and the average values are reported.

2.4. Desorption

Based on the result from the desorption solvent screening, the solvent composition was adjusted to get a mixed methanol/water (3:1, v/v) stabilized with 10 mM AA buffer solution. To study the influence of NaCl on the desorption efficiency, four desorption solvents were prepared with varying NaCl concentrations namely: RS1 (no salt), RS2 (10 mM NaCl), RS3 (50 mM NaCl) and RS4 (500 mM NaCl). After 72 h of adsorption, the adsorbent was recovered by filtration and placed respectively in 20 mL desorption solvent containing the above NaCl concentrations to be continuously stirred for another 72 h at room temperature. The sample mass used for desorption was assumed the same with the initial mass. Sample preparation for NMR analysis followed the steps mentioned previously.

2.5. Hydrothermal synthesis of MOF

MIL-96 was synthesized according to the original method described previously (Loiseau et al., 2006) whereas the protocol for polymer addition was adapted from another study (Nandiyanto et al., 2019). A typical hydrothermal synthesis solution contains $Al(NO_3)_3 \cdot 9H_2O$ (1.3 g, 3.5 mmol), TMA (0.1 g, 0.5 mmol) and H_2O (5 mL, 278 mmol) in a 23 mL Teflon liner. Firstly, to induce particle aggregation, HPAM solution (1000 mg/L) was poured into the reacting solution containing only the dissolved linker in H_2O. The solution was later sonicated for 15 minutes prior to adding the metal precursor. The ratio between the volume of polymer solutions added and the volume of water (R) is defined in Eq. (1). The mixture was heated to 210 °C for 24 h. After cooling to ambient conditions, the resulting solid product was recovered via filtration and consequently washed with copious amount of H_2O. The washed residue was dried at 120 °C in vacuo overnight. Similar steps were implemented when using other polymer solutions (PAM and PAA). Chemical structures for all the polymers are illustrated in Fig. S1 of the Supplementary Information (SI).

$$R = \frac{Volume\ of\ polymer\ (mL)}{Volume\ of\ water\ used\ as\ solvent\ in\ the\ reaction\ (mL)} \quad 1$$

3. Results and discussion

3.1. SEM

For MIL-96, HPAM is proven effective in changing the MOF particle morphology as observed in Fig. 1a − 1d. Generally, starting from the normally reported small hexagonal bipyramidal shaped (HB) crystals (Benzaqui et al., 2017), higher HPAM concentrations facilitate incremental increases in the aspect ratio (length: diameter), transitioning from hexagonal spindles (HS) to elongated hexagonal rods (HR), particularly when 20 mL HPAM was used (MIL-96-RHPAM2). Upon closer inspection from out-of-plane PXRD measurements, the apparent HS morphology was revealed to be a hybrid form of two elongated hexagonal pyramids seamlessly connected at the long axis (Sindoro et al., 2013).

It was reported that the hydrothermal synthesis conditions for MIL-96 must be strictly controlled given the possibility of forming two larger pore Al trimesates, MIL-100 and MIL-110, in the same reaction system despite all having distinct crystal structures. MIL-100 is the kinetically stable product which forms at short reaction times and low pH condition whereas the thermodynamically favored MIL-96 can be obtained after longer reaction times. MIL-110, on the other hand, crystallizes in a much more acidic or basic medium (Haouas et al., 2009). Their corresponding crystal morphologies have also been solved with MIL-96, MIL-100 and MIL-110 presenting a flat hexagonal, an octahedral and a hexagonal needle-like habits respectively (Haouas et al., 2012). Therefore, the influence of HPAM on the crystal morphology agrees well with the stability order of these phases; MIL-96 > MIL-110 > MIL-100.

The addition of HPAM seems to play multiple roles in the crystal elongation phenomenon, firstly as a competing modulator. Since the pK_a value for HPAM (4.5) (Li et al., 2002) is similar to that of TMA ($pK_{a1} = 3.51$, $pK_{a2} = 3.89$, $pK_{a3} = 4.70$), there will be competition with the linker to form coordination bonds with available Al. As a result, nucleation rate slows down and permits slow growth of large MOF crystals (Morris et al., 2017). Secondly, the amine ($-NH_2$) groups in both HPAM and PAM increase the basicity of the reacting solution, providing ideal conditions for the formation of MIL-110 ascribed by the existence of HR crystals. HPAM is a copolymer composed of PAM and PAA. To identify the dominant functional groups responsible to the formation of HR, MIL-96 was synthesized using equivalent concentrations of PAM (Fig. 1e) and PAA (Fig. 1f) separately. Before the reaction, the solutions were very acidic upon addition of PAM (pH = 2), PAA (pH = 2.4) and HPAM (pH = 2.2). Such acidic environment increases the likelihood of $-NH_2$ groups protonating to form primary ammonium ions ($-NH_3^+$) in preference to the ionization of the −COOH groups on the TMA due to higher pK_a values. It is therefore expected to see the $-NH_2$ groups contained in HPAM and PAM to govern the crystal elongation mechanism, transforming the HB shape into the HR habit more so than using PAA.

Following the addition of 20 mL PAA, it is unclear what drives the formation of new hexagonal lumps (HL) with some truncated and larger in dimension among the HR. What might have happened is, from the instant of mixing PAA in water, the dissociated Na^+ cations may end up competing with the Al^{3+} species to form bonds with the linker, causing deceleration in the crystal growth and altering the original template. Another factor that may have undermined PAA's influence is due to its low molecular weight (~2100 g/mol). By substituting higher molecular weight PAA for the synthesis, its influence toward crystal elongation may be amplified.

Finally, the successes in morphological change shown in the MIL-96 samples can be attributed to the solubility of the linker

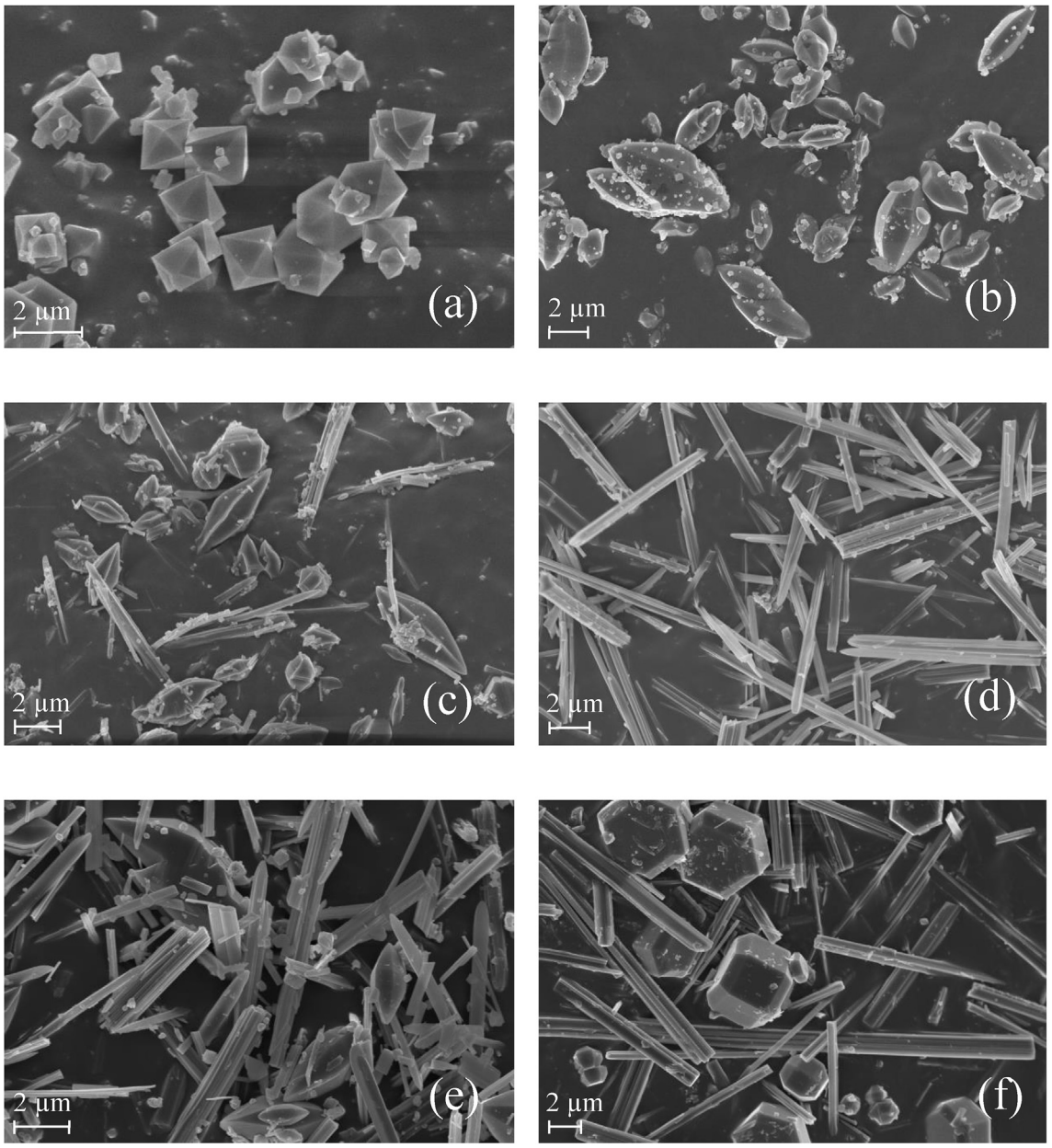

Fig. 1. Modified MIL-96 crystals with (a) no polymer, (b) 2 mL HPAM ($R_{HPAM} = 0.2$), (c) 6 mL HPAM ($R_{HPAM} = 0.6$), (d) 20 mL HPAM ($R_{HPAM} = 2$), (e) 20 mL PAM ($R_{PAM} = 2$), and (f) 20 mL PAA ($R_{PAA} = 2$).

(TMA) in water. Simultaneous dissolution of both TMA and HPAM during the pre-mixing stage facilitates smooth integration of the latter species into the reacting solution, which subsequently changes the MOF crystal morphology. On a side note, identical experiments were performed involving similar modification of another MOF. Readers are referred to Fig. S2 – S4 in the SI for further information.

3.2. PXRD

As shown in Fig. 2, the PXRD patterns of every sample are slightly different compared to the simulated MIL-96 spectra. The peaks have also been shifted slightly to higher angle. The drift may be attributed to the presence of free TMA inside the pores of the samples (Abid et al., 2016). The aforementioned series of crystal shape changes can be defined using the Bravais, Frisdel, Donnay and Harker (BFDH) theory which describes the three main planes that make up the morphology of MIL-96; they are (002), (100) and (101) at $2\theta = 5.7°$, 7.1° and 7.7° respectively (Liu et al., 2015a). Except for the subtly present (002), other key characteristic peaks including (102), match well with the simulated spectra, indicating the core crystalline structure is retained. Although by visual inspection, MIL-110 was mainly present at higher HPAM loading as evident by the HR formation, due to instrument limitation (minimum $2\theta \geq 5°$), the characteristic XRD peaks of MIL-100 ($2\theta = 4°$) and MIL-110 ((001) facet; $2\theta = 5°$) (Lin et al., 2013) cannot be clearly detected and thus, have to be omitted from subsequent discussion.

With higher concentration of HPAM, the emerging (100) facet indicates it could enhance the growth rate of the (100), resulting in narrowed edge and the lengthening of the crystals. Furthermore, higher proportion of HPAM accentuates the growth of the (101) crystal plane as shown by the gradual peak increase in which

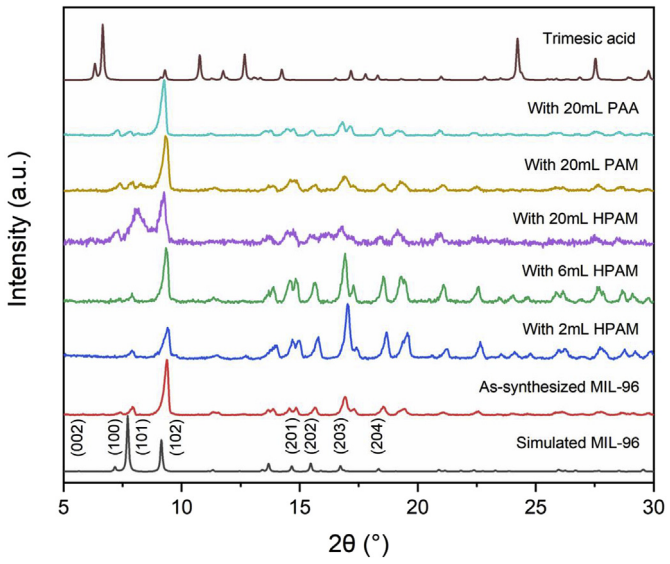

Fig. 2. PXRD patterns of the simulated MIL-96 compared to the as-synthesized MIL-96 samples modified with different types and proportions of polymers.

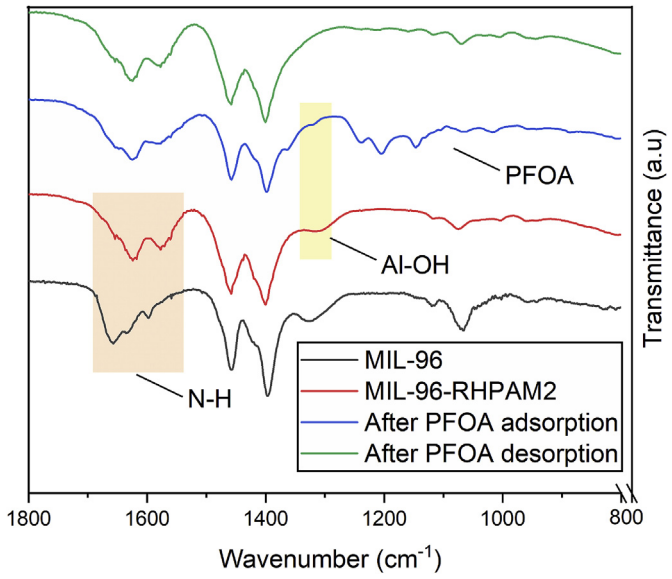

Fig. 3. FTIR spectra for the parent MIL-96 and MIL-96-RHPAM2 before and after PFOA adsorption.

alongside with (100), completes the formation of HR crystal morphology. This is consistent with the reported SEM images. The $-NH_2$ groups in HPAM function like OH^- ions, increasing solution basicity and speeding up the growth rate along the (101) facet, consequently forming the HR habit (Lin et al., 2013).

After the addition of PAA, the (002) facet that is responsible for the formation of HL is only weakly observed in the PXRD, as with the simulated MIL-96, which is probably affected by instrument background noise during scanning, impure phase with ill-defined morphology and powder size inconsistency. Although the BFDH theory also states that the growth rate of the (002) facet to be relatively unaffected, the number of products containing the (002) plane may be subservient compared to the bulk phase which is dominated with (100) and (101)-directed crystals. In short, the preferential crystal growth along the (100) and (101) planes, as a function of higher polymer concentrations, transformed the crystal anisotropy by promoting crystal elongation from its original HB shape. For a hexagonal lattice system, the impact of polymer presence in the reacting environment accelerated the growth along the *c* axis (Sindoro et al., 2013). Moreover, with a higher quantity of added polymers, the subtle width broadening of the strongest peak corresponding to the (102) crystal face implies a slight decrease in particle size. In addition, the relative Bragg peaks of (200) and (201) also become broader and less intense compared to the original MIL-96, supporting the minor reduction in particle size and crystallinity.

3.3. FTIR

FTIR spectroscopy was used to understand PFOA adsorption mechanism onto MIL-96-RHPAM2 and the linker interaction with added polymer (Fig. S5). Detailed analysis of the IR peaks is displayed in Table S1. The collected spectra of spent MIL-96-RHPAM2 in Fig. 3 confirms that PFOA was adsorbed through electrostatic interaction with the MOF. A previous study also inferred the increased intensities of symmetric (v_s) to asymmetric (v_{as}) COO^- stretch after PFOA adsorption in relation to an inner-sphere complexation with the metal centers. In this case, the carboxylate head groups of PFOA may have formed electrostatic bonds to the surface of MIL-96-RHPAM2 (Gao and Chorover, 2012). The consistent N–H peak on both spectra of MIL-96-RHPAM2 after PFOA adsorption and desorption indicates minimal leaching of the HPAM functionality.

3.4. BET

The use of PAM, PAA and HPAM for this particle size modification led to a significant reduction in the apparent surface area (SA_{BET}), see Fig. S6. The pore size distribution plot in Fig. S7 clearly proves complete pore blocking when HPAM was used, asserting its location inside the pores. Interestingly, compared to the apparent surface area of AC (SA_{BET} = 1179 m^2/g), MIL-96-RHPAM2 (SA_{BET} = 75 m^2/g) has comparatively good PFOA adsorption capacity even though it possesses a lower surface area.

3.5. Adsorption kinetics

Apart from knowing the equilibrium adsorption capacity of sorbents (Fig. S10), it is equally important to understand the adsorption kinetics involved in the PFOA removal by MIL-96-RHPAM2. Based on previous studies, the experimental data obtained herein is fitted using a pseudo second order (PSO) kinetic model. Fig. S12 highlights the severe diffusion limitation exhibited by MIL-96-RHPAM2 as the material's adsorptive capacity only reached its plateau after 186 h of contact time. Concurrently, the PFOA adsorption data can also be described by the Elovich kinetic model. Non-linear plots using both models showed high regression coefficients with PSO (R^2 = 0.983) and Elovich (R^2 = 0.996), suggesting chemisorption is the rate limiting step as supported by the FTIR analysis. Since the Elovich equation gave superior approximation to the experimental data, it may be concluded that the adsorption proceeded in a highly heterogenous system (Riahi et al., 2017). Earlier discussions have highlighted the abundance of chemical functional groups comprising of $-NH_2$, $-OH$, $-COOH$, $-NH_3^+$ and the Al^{3+} metal centers on MIL-96-RHPAM2 which may readily bind to PFOA.

To gain a detailed insight in the PFOA adsorption kinetics for MIL-96-RHPAM2, vapor phase adsorption experiments were conducted with a hydrocarbon analogue to PFOA; n-octane (C_8H_{18}) (Fig. S13 – S14). The fundamental differences in liquid-phase adsorption and vapor adsorption are acknowledged but, in both

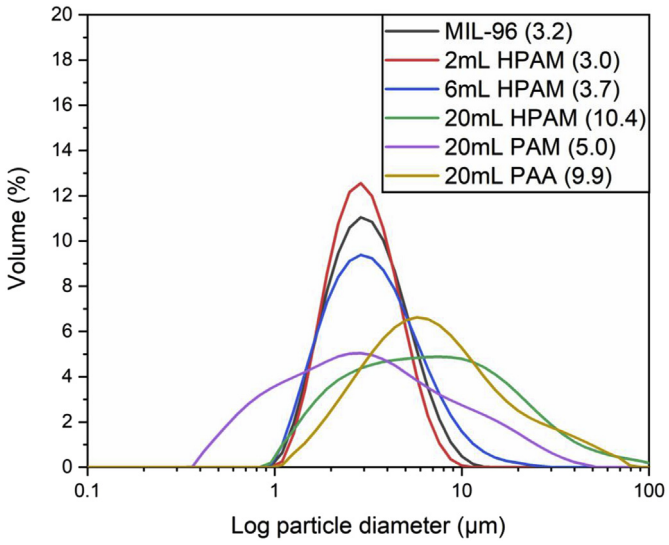

Fig. 4. Measured hydrodynamic particle size distribution (mean volume equivalent sphere diameter in bracket) of polymer-modified MIL-96 in pure water by laser light diffraction (n = 5). The particle size ranges shown reflect the true size as particles were pre-sonicated prior to the laser light diffraction measurement. Addition of 20 mL HPAM effectively formed the largest MIL-96 particles with 225% diameter increase from 3.2 μm to 10.4 μm.

cases, the kinetic rate is nonetheless similar (denoted by the proximity of $k_2 = 2 \times 10^{-4}$ g/mg.min). Vapor phase adsorption time of 1000 minutes is still insufficient to realize an equilibrium adsorption state. The BET result shows that although increasing the HPAM content increases the particle size (Fig. 4), it has compromised the material's porosity. In turn, there is an increase in the diffusion path length inside the adsorbent that hindered effective diffusion and prolonging the time required to reach equilibrium (Kumar et al., 2019). It may appear that the approach outlined here has created another problem but, there is a future opportunity to retain the beneficial effect provided by HPAM by tuning MIL-96 adsorption capacity with temperature, taking into account the high thermal stability of HPAM (Al-Hamairi and AlAmeri, 2020) and the MOF flexibility of changing and increasing its pore size (Barton et al., 2018).

In comparison to the reported kinetic data for PFOA removal by several other adsorbents, MIL-96-RHPAM2 can adsorb PFOA at loading levels on a par with other adsorbents, but the extremely slow uptake would be a significant drawback for its practical use. Relative to other adsorption studies displayed in Table 1, the PFOA concentration used in this work is the highest.

3.6. PFOA adsorption and desorption

Knowing that PFCs are hazardous chemicals, safe regeneration and economical reuse of the spent adsorbents is critically important. Although thermal regeneration is preferably used by carbon manufacturers, adsorbed PFCs are not easily removed from the carbon surfaces by decomposition as C—F is the strongest single bond in organic chemistry after B—F, Si—F and H—F. While the next best alternative is to use higher regeneration temperatures to break the C—F bond, this often results in high carbon losses (Ateia et al., 2019).

To develop an efficient PFOA regeneration method from spent MOF, the nature of adsorption processes must first be understood. An earlier report on PFOA adsorption by MOF had confirmed the electrostatic interaction between the cationic MOF species (Al^{3+}) with the anionic carboxylate groups (COO^-) of PFOA as the main binding mechanism, supplemented by H-bonding and hydrophobic interaction to a lesser extent (Jun et al., 2019). So, with electrostatic interaction being the most prevalent, it was decided to trial saline eluents to evaluate their destabilization effect on the electrostatic PFOA adsorption complex.

The positively charged Al^{3+} center of MIL-96 is surmised to have a strong interaction with the anionic carboxylate groups (COO^-) of PFOA. Contrary to expectations, increasing the eluent ionic strength has minimal effect on PFOA desorption by MIL-96-RHPAM2 (Shih and Wang, 2013; Wang and Shih, 2011) except for a slight drop at the highest tested salt concentration (500 mM NaCl). Such salt concentration may be sufficiently high enough to reduce the electrostatic forces between the Al^{3+} center and the negatively charged PFOA molecules resulting from the competitive PFOA adsorption with the background ions (Na^+ and Cl^-) (Gao and Chorover, 2012). However, due to the well-established acid-base and electrostatic bonds between the Al^{3+}, carboxylate (COO^-), hydroxyl (OH), NH_2 and NH_3^+ functional groups on the MOF, the driving force to establish new bonds with the incoming Na^+ and Cl^- ions is not as favorable, hence, not accommodating the desorption of adsorbed PFOA molecules into the eluent phase.

Apart from the Al^{3+} center being a major MOF binding site, it is probable that the NH_2, which will also exist in a protonated form as a NH_3^+, contained in HPAM also attaches to the anionic carboxylate of PFOA via strong electrostatic adsorption forces (Ali et al., 2020; Deng et al., 2013; Liu et al., 2015b). In addition, the van der Waals interaction between the carbon chain of PFOA (8 carbons on the PFOA) and the main skeleton $(CH_2—CH)_n$ of HPAM may also

Table 1
Comparison of the pseudo-second order kinetic parameters for PFOA adsorption by select MOFs and AC.

Sorbent used	Tested PFOA concentration (mg/L)	Pseudo-second order model parameter			Equilibrium time (hr)	Reference
		q_e (mg/g)	k_2 (g/mg.min)	R^2		
Bamboo-derived AC	120	393	2.7×10^{-5}	0.91	33.5	Du et al. (2015)
Fe_3O_4-modified AC	300	364	7.1×10^{-5}	0.998	29	Xu et al. (2020)
Perfluorinated UiO-66-(F4)	500	381	2.6×10^{-3}	0.993	1	Sini et al. (2018)
UiO-66		327	2.7×10^{-3}	0.996		
MIL-101 (Cr)	100	481	1.4×10^{-4}	0.967	1	Liu et al. (2015b)
Quaternized amine MIL-101 (Cr)-QDMEN		791	2.1×10^{-4}	0.985		
MIL-53 (Al)	1	100	7.3×10^{-2}	0.999	4	Jun et al. (2019)
ZIF-7	–	22	7.1×10^{-5}	0.994	1	Chen et al. (2016)
ZIF-8		177	2.0×10^{-5}	0.978		
ZIF-L		244	9.6×10^{-6}	0.985		
UiO-67	500	350	6.1×10^{-4}	0.999	1	Sini et al. (2019)
MIL-96-RHPAM2	1000	340[a]	1.7×10^{-4}	0.983	186	This work

[a] Shows the increase in adsorption capacity after kinetic experiment was extended to 186 h suggesting MIL-96-RHPAM2 has a very slow kinetic rate.

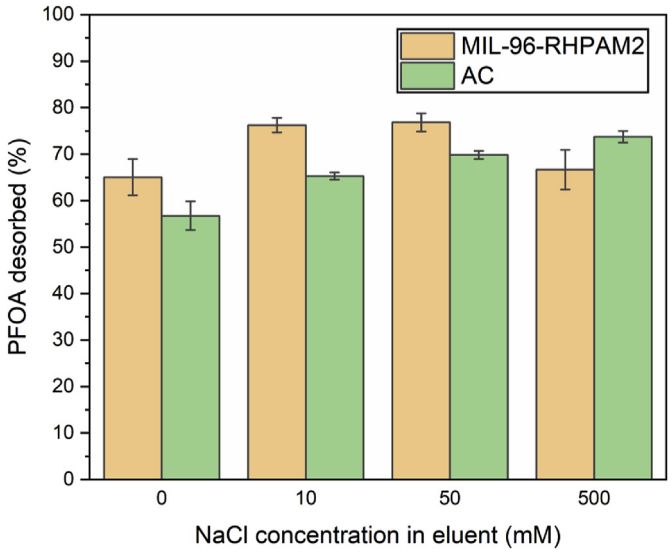

Fig. 5. Percentage of PFOA desorbed from MIL-96-RHPAM2 and AC using eluents with various NaCl concentrations (temperature 25 °C, adsorbent dose = 2 mg/L, initial PFOA concentration = 1000 mg/L).

contribute to the adsorption process. Altogether, these explanations for the incomplete desorption of PFOA from aminated adsorbents such as MIL-96-RHPAM2 are in line with the obtained result from batch desorption studies. Fig. 5 illustrates the nuanced NaCl influence in the eluent to the PFOA desorption performance of MIL-96-RHPAM2. Across the tested salinity window, the highest PFOA fraction desorbed only reached 77% but not full recovery, providing future research opportunities to clarify the best solvent/salt systems capable of complete PFOA desorption. Descriptions on the possible PFOA adsorption mechanisms onto MIL-96-RHPAM2 can be found in Fig. S16 (Scheme S1) and Fig. S17 (Scheme S2) for the pristine form.

Although PFOA desorption efficiency from AC is inferior to MIL-96-RHPAM2 at lower ionic strengths, AC's desorption efficiency is improved at the highest ionic strength tested here. Similar to MOF, PFOA adsorption onto AC shares similar adsorption mechanisms (Wang and Shih, 2011; Wang et al., 2019), confirming the importance of surface chemistry on AC. There is a clear correlation with a marked increase in PFCs sorption with more availability of basic groups in the adsorbents. Thus, to enhance the adsorption process, an abundance of hydroxyl and carboxyl oxygen-containing functional groups on the AC surface will then interact with the PFOA anions via acid-base/electrostatic interactions (Sun et al., 2016; Zhi and Liu, 2016). Along the same lines, the oxygen-containing basic and acidic surface groups on AC may form H-bond interactions with the amphoteric COOH functional groups within PFOA. An increase in the eluent ionic strength can potentially weaken these PFOA to AC H-bonding interactions by the Na^+ and the Cl^- ions shielding the electrostatic interactions whilst also directly competing for the H-bonding sites. While these results show that NaCl was not an effective PFOA desorption facilitating agent, only catalytic degradation has so far offered superior performance (Du et al., 2014; Zhao et al., 2013).

4. Conclusions

In summary, the addition of an anionic polymer (HPAM) to a cationic aluminum-based MOF (MIL-96) during the hydrothermal synthesis stage allowed the formation of larger MOF crystals with well-defined crystal habits. Taking advantage of HPAM being a low cost and an environmentally friendly additive, a HPAM-modified MIL-96 (MIL-96-RHPAM2) showed promising particle size growth from 3.2 μm to 10.4 μm as well as the ability to control the crystal morphology using this simple modification procedure. Incorporating HPAM into the MIL-96 structure resulted in the introduction of amine functionality, which can form a primary ammonium species that in turn led to improved PFOA adsorption capacity relative to the pristine form, while also promoting higher PFOA affinity compared to AC. Higher concentrations of NaCl in the eluent solvents did not yield enhanced PFOA desorption from both spent adsorbents, MIL-96-RHPAM2 (maximum PFOA desorbed was 77%) and AC (74%), primarily due to the strong PFOA adsorption to both adsorbents.

CRediT author statement

Luqman Hakim Mohd Azmi: Conceptualization, Methodology, Validation, Formal analysis, Investigation, Writing - original draft, Visualization. Daryl R. Williams**:** Conceptualization, Methodology, Resources, Writing - review & editing, Supervision. **Bradley Ladewig:** Conceptualization, Methodology, Resources, Data curation (Zenodo), Writing - review & editing, Visualization (Graphical Abstract and Adsorption Mechanism Schemes), Supervision.

Declaration of competing interest

The authors declare that they have no known competing financial interests or personal relationships that could have appeared to influence the work reported in this paper.

Acknowledgments

Luqman Hakim Mohd Azmi gratefully acknowledges the financial support provided by the sovereign wealth fund of Malaysian Government, Yayasan Khazanah for his PhD studies. The authors also thank Prof. Paul D. Lickiss, Dr. Pavani Cherukupally, Elwin Hunter-Sellars, Dr. Shanxue Jiang and Tingwu Liu for useful discussion on material design and characterization.

Appendix A. Supplementary data

Supplementary data to this article can be found online at https://doi.org/10.1016/j.chemosphere.2020.128072. The raw data presented in all figures, and high-resolution versions of the SEM images, are available from the open repository: https://doi.org/10.5281/zenodo.3813241.

References

Abid, H.R., Rada, Z.H., Shang, J., Wang, S., 2016. Synthesis, characterization, and CO_2 adsorption of three metal-organic frameworks (MOFs): MIL-53, MIL-96, and amino-MIL-53. Polyhedron 120, 103–111.

Al-Hamairi, A., AlAmeri, W., 2020. Development of a novel model to predict HPAM viscosity with the effects of concentration, salinity and divalent content. J. Pet. Explor. Prod. Technol. 1–15.

Ali, M., Meaney, S.P., Giles, L.W., Holt, P., Majumder, M., Tabor, R.F., 2020. Capture of perfluorooctanoic acid using oil-filled graphene oxide–silica hybrid capsules. Environ. Sci. Technol. 54, 3549–3558.

Andersson, E.M., Scott, K., Xu, Y., Li, Y., Olsson, D.S., Fletcher, T., Jakobsson, K., 2019. High exposure to perfluorinated compounds in drinking water and thyroid disease. A cohort study from Ronneby, Sweden. Environ. Res. 176, 108540.

Ateia, M., Attia, M.F., Maroli, A., Tharayil, N., Alexis, F., Whitehead, D.C., Karanfil, T., 2018. Rapid removal of poly-and perfluorinated alkyl substances by poly (ethylenimine)-functionalized cellulose microcrystals at environmentally relevant conditions. Environ. Sci. Technol. Lett. 5, 764–769.

Ateia, M., Maroli, A., Tharayil, N., Karanfil, T., 2019. The overlooked short-and ultrashort-chain poly-and perfluorinated substances: a review. Chemosphere 220, 866–882.

Azhar, M.R., Abid, H.R., Tade, M.O., Periasamy, V., Sun, H., Wang, S., 2018. Cascade applications of robust MIL-96 metal organic frameworks in environmental

remediation: proof of concept. Chem. Eng. J. 341, 262–271.
Badruddoza, A.Z.M., Bhattarai, B., Suri, R.P.S., 2017. Environmentally friendly β-cyclodextrin–ionic liquid polyurethane-modified magnetic sorbent for the removal of PFOA, PFOS, and Cr (VI) from water. ACS Sustain. Chem. Eng. 5, 9223–9232.
Barton, H.F., Davis, A.K., Lee, D.T., Parsons, G.N., 2018. Solvothermal synthesis of MIL-96 and UiO-66-NH_2 on atomic layer deposited metal oxide coatings on fiber mats. J. Vis. Exp. e57734. https://doi.org/10.3791/57734.
Benzaqui, M., Pillai, R.S., Sabetghadam, A., Benoit, V., Normand, P., Marrot, J., Menguy, N., Montero, D., Shepard, W., Tissot, A., 2017. Revisiting the aluminum trimesate-based MOF (MIL-96): from structure determination to the processing of mixed matrix membranes for CO_2 capture. Chem. Mater. 29, 10326–10338.
Chang, Y., Huang, H., Wang, L., Li, Y., Zhong, C., 2020. Synergistic dual-Li+ sites for CO_2 separation in metal-organic framework composites. Chem. Eng. J. 402 (126201), 1–9. https://doi.org/10.1016/j.cej.2020.126201.
Chen, X., Vanangamudi, A., Wang, J., Jegatheesan, J., Mishra, V., Sharma, R., Gray, S.R., Kujawa, J., Kujawski, W., Wicaksana, F., Dumée, L.F., 2020. Direct contact membrane distillation for effective concentration of perfluoroalkyl substances - Impact of surface fouling and material stability. Water Res. 182 (116010), 1–10. https://doi.org/10.1016/j.wares.2020.116010.
Chen, M.-J., Yang, A.-C., Wang, N.-H., Chiu, H.-C., Li, Y.-L., Kang, D.-Y., Lo, S.-L., 2016. Influence of crystal topology and interior surface functionality of metal-organic frameworks on PFOA sorption performance. Microporous Mesoporous Mater. 236, 202–210.
Cordner, A., Vanessa, Y., Schaider, L.A., Rudel, R.A., Richter, L., Brown, P., 2019. Guideline levels for PFOA and PFOS in drinking water: the role of scientific uncertainty, risk assessment decisions, and social factors. J. Expo. Sci. Environ. Epidemiol. 29, 157.
Deng, S., Niu, L., Bei, Y., Wang, B., Huang, J., Yu, G., 2013. Adsorption of perfluorinated compounds on aminated rice husk prepared by atom transfer radical polymerization. Chemosphere 91, 124–130. https://doi.org/10.1016/j.chemosphere.2012.11.015.
Du, Z., Deng, S., Bei, Y., Huang, Q., Wang, B., Huang, J., Yu, G., 2014. Adsorption behavior and mechanism of perfluorinated compounds on various adsorbents—a review. J. Hazard Mater. 274, 443–454.
Du, Z., Deng, S., Chen, Y., Wang, B., Huang, J., Wang, Y., Yu, G., 2015. Removal of perfluorinated carboxylates from washing wastewater of perfluorooctanesulfonyl fluoride using activated carbons and resins. J. Hazard Mater. 286, 136–143.
Edomwonyi-Otu, L.C., Adelakun, D.O., 2018. Effect of heavy molecular weight polymer on quality of drinking water. Mater. Today Commun 15, 337–343.
Falcaro, P., Hill, A.J., Nairn, K.M., Jasieniak, J., Mardel, J.I., Bastow, T.J., Mayo, S.C., Gimona, M., Gomez, D., Whitfield, H.J., 2011. A new method to position and functionalize metal-organic framework crystals. Nat. Commun. Now. 2, 237.
Feng, X., Ye, M., Li, Y., Zhou, J., Sun, B., Zhu, Y., Zhu, L., 2020. Potential sources and sediment-pore water partitioning behaviors of emerging per/polyfluoroalkyl substances in the South Yellow Sea. J. Hazard Mater. 389, 122124.
Gagliano, E., Sgroi, M., Falciglia, P.P., Vagliasindi, F.G.A., Roccaro, P., 2020. Removal of poly-and perfluoroalkyl substances (PFAS) from water by adsorption: role of PFAS chain length, effect of organic matter and challenges in adsorbent regeneration. Water Res. 171, 115381.
Gao, X., Chorover, J., 2012. Adsorption of perfluorooctanoic acid and perfluorooctanesulfonic acid to iron oxide surfaces as studied by flow-through ATR-FTIR spectroscopy. Environ. Chem. 9, 148–157.
Gebald, C., Repond, N., Ruesch, T., Wurzbacher, J.A., 2019. Low-pressure drop structure of particle adsorbent bed for adsorption gas separation process. US10427086B2.
Guo, C., Zhang, Y., Guo, Y., Zhang, L., Zhang, Y., Wang, J., 2018. A general and efficient approach for tuning the crystal morphology of classical MOFs. Chem. Commun. 54, 252–255.
Han, Y., Liu, M., Li, K., Zuo, Y., Wei, Y., Xu, S., Zhang, G., Song, C., Zhang, Z., Guo, X., 2015. Facile synthesis of morphology and size-controlled zirconium metal–organic framework UiO-66: the role of hydrofluoric acid in crystallization. CrystEngComm 17, 6434–6440.
Haouas, M., Volkringer, C., Loiseau, T., Ferey, G., Taulelle, F., 2009. The extra-framework sub-lattice of the metal–organic framework MIL-110: a solid-state NMR investigation. Chem. Eur. J. 15, 3139–3146.
Haouas, M., Volkringer, C., Loiseau, T., Férey, G., Taulelle, F., 2012. In situ NMR, ex situ XRD and SEM study of the hydrothermal crystallization of nanoporous aluminum trimesates MIL-96, MIL-100, and MIL-110. Chem. Mater. 24, 2462–2471. https://doi.org/10.1021/cm300439e.
Hu, X.C., Andrews, D.Q., Lindstrom, A.B., Bruton, T.A., Schaider, L.A., Grandjean, P., Lohmann, R., Carignan, C.C., Blum, A., Balan, S.A., 2016. Detection of poly-and perfluoroalkyl substances (PFASs) in US drinking water linked to industrial sites, military fire training areas, and wastewater treatment plants. Environ. Sci. Technol. Lett. 3, 344–350.
Huang, M., Jiao, J., Zhuang, P., Chen, X., Wang, J., Zhang, Y., 2018. Serum polyfluoroalkyl chemicals are associated with risk of cardiovascular diseases in national US population. Environ. Int. 119, 37–46.
Jun, B.-M., Hwang, H.S., Heo, J., Han, J., Jang, M., Sohn, J., Park, C.M., Yoon, Y., 2019. Removal of selected endocrine-disrupting compounds using Al-based metal organic framework: performance and mechanism of competitive adsorption. J. Ind. Eng. Chem. 79, 345–352.
Kumar, P.S., Korving, L., Keesman, K.J., van Loosdrecht, M.C.M., Witkamp, G.-J., 2019. Effect of pore size distribution and particle size of porous metal oxides on phosphate adsorption capacity and kinetics. Chem. Eng. J. 358, 160–169.
Lee, J., Kwak, S.-Y., 2017. Tubular superstructures composed of α-Fe_2O_3 nanoparticles from pyrolysis of metal–organic frameworks in a confined space: effect on morphology, particle size, and magnetic properties. Cryst. Growth Des. 17, 4496–4500.
Li, L., Zheng, H., Wang, T., Cai, M., Wang, P., 2018. Perfluoroalkyl acids in surface seawater from the North Pacific to the Arctic ocean: contamination, distribution and transportation. Environ. Pollut. 238, 168–176.
Li, W., Zhao, H., Teasdale, P.R., John, R., Zhang, S., 2002. Synthesis and characterisation of a polyacrylamide–polyacrylic acid copolymer hydrogel for environmental analysis of Cu and Cd. React. Funct. Polym. 52, 31–41.
Lin, Y., Kong, C., Chen, L., 2013. Facile synthesis of aluminum-based metal-organic frameworks with different morphologies and structures through an OH–assisted method. Chem. Asian J. 8, 1873–1878. https://doi.org/10.1002/asia.201300135.
Liu, D., Liu, Y., Dai, F., Zhao, J., Yang, K., Liu, C., 2015a. Size-and morphology-controllable synthesis of MIL-96 (Al) by hydrolysis and coordination modulation of dual aluminium source and ligand systems. Dalton Trans. 44, 16421–16429.
Liu, K., Zhang, S., Hu, X., Zhang, K., Roy, A., Yu, G., 2015b. Understanding the adsorption of PFOA on MIL-101 (Cr)-based anionic-exchange metal–organic frameworks: comparing DFT calculations with aqueous sorption experiments. Environ. Sci. Technol. 49, 8657–8665.
Loiseau, T., Lecroq, L., Volkringer, C., Marrot, J., Férey, G., Haouas, M., Taulelle, F., Bourrelly, S., Llewellyn, P.L., Latroche, M., 2006. MIL-96, a porous aluminum trimesate 3D structure constructed from a hexagonal network of 18-membered rings and μ3-oxo-centered trinuclear units. J. Am. Chem. Soc. 128, 10223–10230. https://doi.org/10.1021/ja0621086.
Long, P., Wu, H., Zhao, Q., Wang, Y., Dong, J., Li, J., 2011. Solvent effect on the synthesis of MIL-96 (Cr) and MIL-100 (Cr). Microporous Mesoporous Mater. 142, 489–493.
Lorenzo, M., Campo, J., Suárez-Varela, M.M., Picó, Y., 2019. Occurrence, distribution and behavior of emerging persistent organic pollutants (POPs) in a Mediterranean wetland protected area. Sci. Total Environ. 646, 1009–1020.
Mancini, F.R., Cano-Sancho, G., Gambaretti, J., Marchand, P., Boutron-Ruault, M., Severi, G., Arveux, P., Antignac, J., Kvaskoff, M., 2020. Perfluorinated alkylated substances serum concentration and breast cancer risk: evidence from a nested case-control study in the French E3N cohort. Int. J. Canc. 146, 917–928.
Mandic, M., Todic, B., Zivanic, L., Nikacevic, N., Bukur, D.B., 2017. Effects of catalyst activity, particle size and shape, and process conditions on catalyst effectiveness and methane selectivity for Fischer–Tropsch reaction: a modeling study. Ind. Eng. Chem. Res. 56, 2733–2745.
McNamara, J.D., Franco, R., Mimna, R., Zappa, L., 2018. Comparison of activated carbons for removal of perfluorinated compounds from drinking water. Journal-American Water Work. Assoc, 110, E2–E14.
Morris, W., Wang, S., Cho, D., Auyeung, E., Li, P., Farha, O.K., Mirkin, C.A., 2017. Role of modulators in controlling the colloidal stability and polydispersity of the UiO-66 metal–organic framework. ACS Appl. Mater. Interfaces 9, 33413–33418.
Nandiyanto, A.B.D., He, X., Wang, W.-N., 2019. Colloid-assisted growth of metal-organic framework nanoparticles. CrystEngComm 1, 2268–2272. https://doi.org/10.1039/c9ce00033j.
Piekarski, D.J., Diaz, K.R., McNerney, M.W., 2020. Perfluoroalkyl chemicals in neurological health and disease: human concerns and animal models. Neurotoxicology.
Rashtian, J., Chavkin, D.E., Merhi, Z., 2019. Water and soil pollution as determinant of water and food quality/contamination and its impact on female fertility. Reprod. Biol. Endocrinol. 17, 5.
Rellegadla, S., Prajapat, G., Agrawal, A., 2017. Polymers for enhanced oil recovery: fundamentals and selection criteria. Appl. Microbiol. Biotechnol. 101, 4387–4402.
Riahi, K., Chaabane, S., Thayer, B., Ben, 2017. A kinetic modeling study of phosphate adsorption onto Phoenix dactylifera L. date palm fibers in batch mode. J. Saudi Chem. Soc, 21, S143–S152.
Richardson, S.D., 2008. Environmental mass spectrometry: emerging contaminants and current issues. Anal. Chem. 80, 4373–4402. https://doi.org/10.1021/ac202903d.
Rivera-Utrilla, J., Sánchez-Polo, M., Ferro-García, M.Á., Prados-Joya, G., Ocampo-Pérez, R., 2013. Pharmaceuticals as emerging contaminants and their removal from water. A review. Chemosphere 93, 1268–1287. https://doi.org/10.1016/j.chemosphere.2013.07.059.
Scher, D.P., Kelly, J.E., Huset, C.A., Barry, K.M., Hoffbeck, R.W., Yingling, V.L., Messing, R.B., 2018. Occurrence of perfluoroalkyl substances (PFAS) in garden produce at homes with a history of PFAS-contaminated drinking water. Chemosphere 196, 548–555.
Seoane, B., Castellanos, S., Dikhtiarenko, A., Kapteijn, F., Gascon, J., 2016. Multi-scale crystal engineering of metal organic frameworks. Coord. Chem. Rev. 307, 147–187.
Shih, K., Wang, F., 2013. Adsorption behavior of perfluorochemicals (PFCs) on boehmite: influence of solution chemistry. Procedia Environ. Sci. 18, 106–113.
Sindoro, M., Jee, A.Y., Granick, S., 2013. Shape-selected colloidal MOF crystals for aqueous use. Chem. Commun. 49, 9576–9578. https://doi.org/10.1039/c3cc45935g.
Sini, K., Bourgeois, D., Idouhar, M., Carboni, M., Meyer, D., 2019. Metal-organic frameworks cavity size effect on the extraction of organic pollutants. Mater. Lett. 250, 92–95.

Sini, K., Bourgeois, D., Idouhar, M., Carboni, M., Meyer, D., 2018. Metal-organic framework sorbents for the removal of perfluorinated compounds in an aqueous environment. New J. Inside Chem. 42, 17889–17894. https://doi.org/10.1039/c8nj03312a.

Sun, B., Ma, J., Sedlak, D.L., 2016. Chemisorption of perfluorooctanoic acid on powdered activated carbon initiated by persulfate in aqueous solution. Environ. Sci. Technol. 50, 7618–7624.

Sunderland, E.M., Hu, X.C., Dassuncao, C., Tokranov, A.K., Wagner, C.C., Allen, J.G., 2019. A review of the pathways of human exposure to poly-and perfluoroalkyl substances (PFASs) and present understanding of health effects. J. Expo. Sci. Environ. Epidemiol. 29, 131–147.

Tiedeken, E.J., Tahar, A., McHugh, B., Rowan, N.J., 2017. Monitoring, sources, receptors, and control measures for three European Union watch list substances of emerging concern in receiving waters – a 20 year systematic review. Sci. Total Environ. 574, 1140–1163. https://doi.org/10.1016/j.scitotenv.2016.09.084.

Vaitsis, C., Sourkouni, G., Argirusis, C., 2019. Metal organic frameworks (MOFs) and ultrasound: a review. Ultrason. Sonochem. 52, 106–119.

Valsecchi, S., Conti, D., Crebelli, R., Polesello, S., Rusconi, M., Mazzoni, M., Preziosi, E., Carere, M., Lucentini, L., Ferretti, E., 2017. Deriving environmental quality standards for perfluorooctanoic acid (PFOA) and related short chain perfluorinated alkyl acids. J. Hazard Mater. 323, 84–98.

Vecitis, C.D., Park, H., Cheng, J., Mader, B.T., Hoffmann, M.R., 2009. Treatment technologies for aqueous perfluorooctanesulfonate (PFOS) and perfluorooctanoate (PFOA). Front. Environ. Sci. Eng. China 3, 129–151.

Wang, F., Guo, H., Chai, Y., Li, Y., Liu, C., 2013. The controlled regulation of morphology and size of HKUST-1 by "coordination modulation method.". Microporous Mesoporous Mater. 173, 181–188.

Wang, F., Shih, K., 2011. Adsorption of perfluorooctanesulfonate (PFOS) and perfluorooctanoate (PFOA) on alumina: influence of solution pH and cations. Water Res. 45, 2925–2930.

Wang, W., Mi, X., Shi, H., Zhang, X., Zhou, Z., Li, C., Zhu, D., 2019. Adsorption behaviour and mechanism of the PFOS substitute OBS (sodium p-perfluorous nonenoxybenzene sulfonate) on activated carbon. R. Soc. Open Sci. 6, 191069.

Wang, Z., DeWitt, J.C., Higgins, C.P., Cousins, I.T., 2017. A never-ending story of per- and polyfluoroalkyl substances (PFASs)? Environ. Sci. Technol. 51, 2508–2518.

Watanabe, S., Ohsaki, S., Hanafusa, T., Takada, K., Tanaka, H., Mae, K., Miyahara, M.T., 2017. Synthesis of zeolitic imidazolate framework-8 particles of controlled sizes, shapes, and gate adsorption characteristics using a central collision-type microreactor. Chem. Eng. J. 313, 724–733.

Xiao, L., Ling, Y., Alsbaiee, A., Li, C., Helbling, D.E., Dichtel, W.R., 2017. β-Cyclodextrin polymer network sequesters perfluorooctanoic acid at environmentally relevant concentrations. J. Am. Chem. Soc. 139, 7689–7692. https://doi.org/10.1021/jacs.7b02381.

Xu, J., Liu, Z., Zhao, D., Gao, N., Fu, X., 2020. Enhanced adsorption of perfluorooctanoic acid (PFOA) from water by granular activated carbon supported magnetite nanoparticles. Sci. Total Environ. 723 (137757), 1–9. https://doi.org/10.1016/j.scitotenv.2020.137757.

Xue, H., Chen, Q., Jiang, F., Yuan, D., Lv, G., Liang, L., Liu, L., Hong, M., 2016. A regenerative metal–organic framework for reversible uptake of Cd (II): from effective adsorption to in situ detection. Chem. Sci. 7, 5983–5988.

Yan, X., Lu, N., Fan, B., Bao, J., Pan, D., Wang, M., Li, R., 2015. Synthesis of mesoporous and tetragonal zirconia with inherited morphology from metal–organic frameworks. CrystEngComm 17, 6426–6433.

Yang, Y., Ding, Q., Yang, M., Wang, Y., Liu, N., Zhang, X., 2018. Magnetic ion exchange resin for effective removal of perfluorooctanoate from water: study of a response surface methodology and adsorption performances. Environ. Sci. Pollut. Res. 25, 29267–29278.

Zhao, H., Gao, J., Zhao, G., Fan, J., Wang, Yanbin, Wang, Yujing, 2013. Fabrication of novel SnO_2-Sb/carbon aerogel electrode for ultrasonic electrochemical oxidation of perfluorooctanoate with high catalytic efficiency. Appl. Catal. B Environ. 136–137, 278–286. https://doi.org/10.1016/j.apcatb.2013.02.013.

Zhi, Y., Liu, J., 2016. Surface modification of activated carbon for enhanced adsorption of perfluoroalkyl acids from aqueous solutions. Chemosphere 144, 1224–1232. https://doi.org/10.1016/j.chemosphere.2015.09.097.